ACS APPLIED MATERIALS & INTERFACES

Research Article

www.acsami.org

Kesterite $Cu_2ZnSn(S,Se)_4$ Solar Cells with beyond 8% Efficiency by a Sol–Gel and Selenization Process

Fangyang Liu,*[,†,‡] Fangqin Zeng,[†] Ning Song,[‡] Liangxing Jiang,[†] Zili Han,[†] Zhenghua Su,[†] Chang Yan,[‡] Xiaoming Wen,[‡] Xiaojing Hao,*[,‡] and Yexiang Liu[†]

[†]School of Metallurgy and Environment, Central South University, Changsha, Hunan 410083, China

[‡]School of Photovoltaic and Renewable Energy Engineering, University of New South Wales, Sydney, New South Wales 2052, Australia

Supporting Information

ABSTRACT: A facile sol–gel and selenization process has been demonstrated to fabricate high-quality single-phase earth abundant kesterite $Cu_2ZnSn(S,Se)_4$ (CZTSSe) photovoltaic absorbers. The structure and band gap of the fabricated CZTSSe can be readily tuned by varying the [S]/([S] + [Se]) ratios via selenization condition control. The effects of [S]/([S] + [Se]) ratio on device performance have been presented. The best device shows 8.25% total area efficiency without antireflection coating. Low fill factor is the main limitation for the current device efficiency compared to record efficiency device due to high series resistance and interface recombination. By improving film uniformity, eliminating voids, and reducing the $Mo(S,Se)_2$ interfacial layer, a further boost of the device efficiency is expected, enabling the proposed process for fabricating one of the most promising candidates for kesterite solar cells.

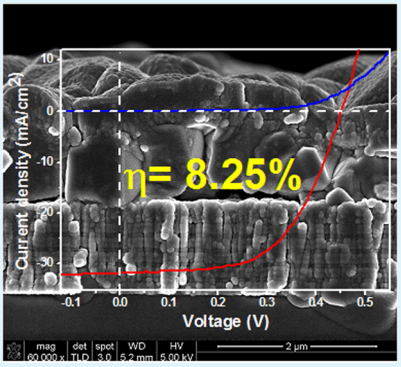

KEYWORDS: *kesterite, $Cu_2ZnSn(S,Se)_4$, thin film solar cells, sol–gel, interface recombination*

1. INTRODUCION

Kesterite $Cu_2ZnSn(S,Se)_4$ (CZTSSe) semiconductor has attracted worldwide attention due to its excellent optical and electronic properties compared to traditional $Cu(In,Ga)Se_2$ (CIGS) and CdTe materials for thin film solar cells while consisting of earth-abundant and low-toxic constituent elements. Remarkable progress has been made in CZTSSe solar cells over the past few years, and the highest efficiency (PCE, 12.6%) has been achieved by IBM group[1] showing substantial commercial promise.

Similar to CIGS, CZTSSe thin films can be fabricated by both vacuum and solution processes. For vacuum based processes, over 9% efficiencies of $Cu_2ZnSnSe_4$ (CZTSe) devices have been realized by coevaporation[2,3] which is an in situ growth process allowing real-time control in chemical composition and reaction path. Cu_2ZnSnS_4 (CZTS) devices from evaporated precursors and sulfurization have yielded efficiencies above 8%.[4,5] The annealing of sputtered precursors under reactive atmosphere containing S_2[6] or H_2Se[7] has also created devices with efficiencies beyond 9%. For solution-based processes, they can be subdivided into electrodeposition, nanoparticle ink coating, and pure solution coating approaches. Devices from electrodeposited metallic precursors followed by sulfurization and selenization have achieved 8%[8] and 7%[9] efficiencies, respectively. Several successful investigations based on nanoparticle ink coating followed by chalcogenization annealing have been reported reaching 8.5% from mixed binary and ternary nanoparticles,[10] 9.0% from quaternary CZTS nanocrystals,[11] 8.4% from Ge-incorporated CZTS nanocrystals,[12] and 5.14% in aqueous nanoinks.[13] It is worth noting that a series of record-setting devices have been developed by IBM group using a hydrazin-based hybrid solution–particle slurry process.[14−16] In contrast with all aforementioned technologies, pure solution approach offers precursors homogeneity at a molecular scale and accordingly enables precise stoichiometric control and excellent film consistency, which are necessary for low-cost and large-scale production. A number of attractive efficiencies for CZTSSe cells have been achieved based on various solvents: 8.08% by hydrazine-hydrazinocarboxylic acid dissolution of Zn metal,[17] 6.13% by water–ethanol,[18] 6.03% by ethanol–CS_2–1-butylamine-thioglycolic acid,[19] 8.32% by dimethyl sulfoxide (DMSO),[20] and 12.6% by hydrazine (record efficiency).[1]

Our group previously reported a facile molecular pure solution route to fabricate sulfide CZTS thin films by a sol–gel and sulfurization process, producing CZTS solar cell with efficiency of 5.1%,[21] which was then improved to 5.7% by low-pressure sulfurization.[22] Our sol solution was made by dissolving Cu, Zn, and Sn salts and excess thiourea in 2-methoxyethanol. Thiourea was added into the solvent to form metal-thiourea-oxygen complex with metal ions, then the complexes were thermally decomposed into CZTS xerogel

Received: February 5, 2015
Accepted: June 16, 2015
Published: June 16, 2015

DOI: 10.1021/acsami.5b01151
ACS Appl. Mater. Interfaces 2015, 7, 14376−14383

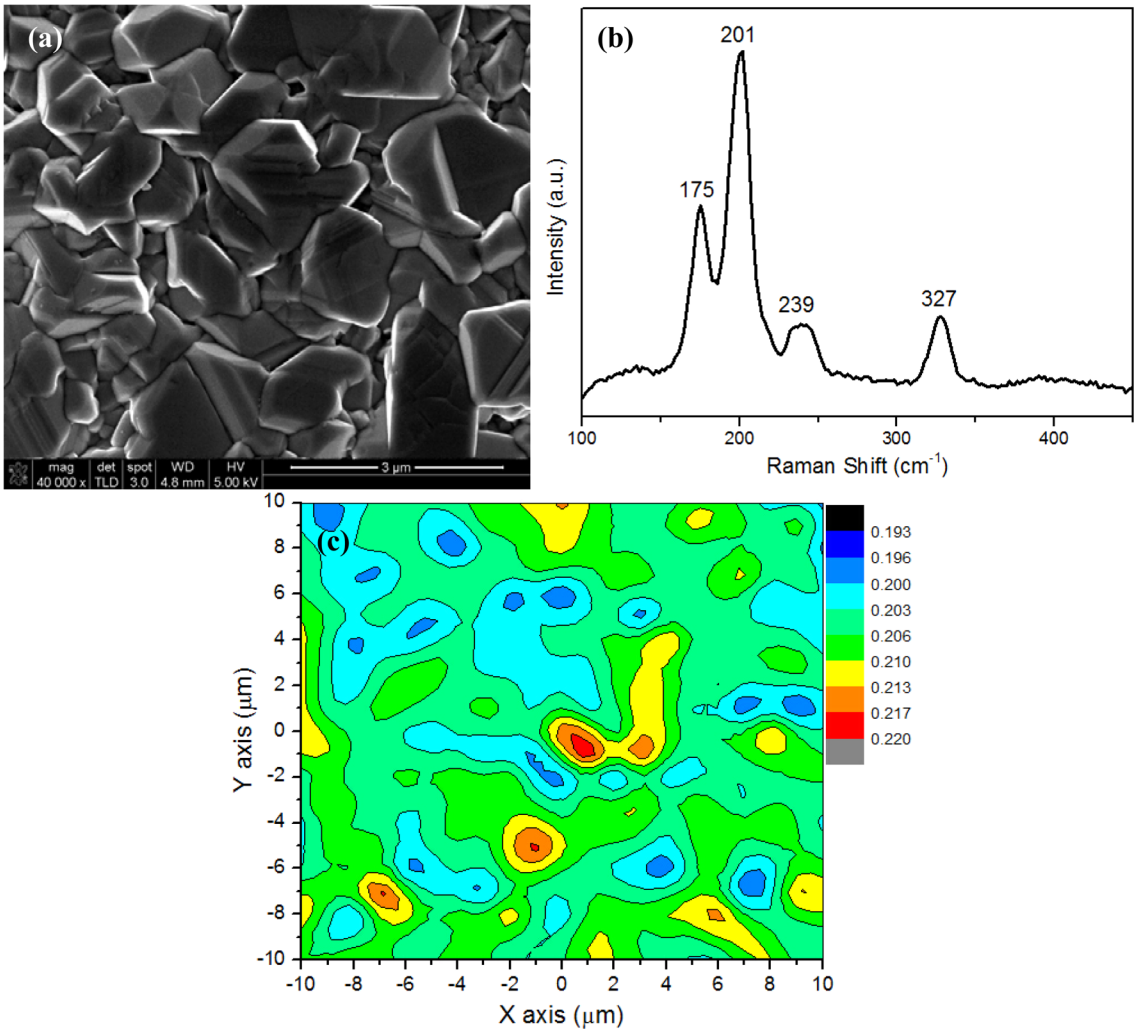

Figure 1. (a) Typical SEM top view and (b) Raman spectrum of the typical CZTSSe absorber. (c) Raman mapping representing the ratio of the peak intensity for sulfide and selenide peaks after background subtracting.

precursor films during air annealing.[21] This is different from conventional sol–gel processes, which entail forming metal–oxygen–metal bonds in sol solution and metal oxides in gel film[23,24] and the need for highly reactive but toxic H_2S in postsulfurization process for sulfides formation.[25,26] Here, employing the same CZTS xerogel precursor materials, we present an approach to fabricate sulfoselenide CZTSSe absorbers by postselenization and report the solar cell device with a total-area efficiency of 8.2% without antireflection coating. The capability to control [S]/([S] + [Se]) ratio and resulting structural and optoelectronic properties of the absorbers by adjusting the selenium partial pressure during selenization has also been demonstrated.

2. EXPERIMENTAL SECTION

2.1. Precursor Sol Solution Preparation. The precursor solution was prepared by dissolving $Cu(CH_3COO)_2{\cdot}H_2O$ (0.46 mol/L, AR), $Zn(CH_3COO)_2{\cdot}2H_2O$ (0.27 mol/L, AR), $SnCl_2{\cdot}2H_2O$ (0.27 mol/L, AR), and $SC(NH_2)_2$ (2 mol/L, AR) into 2-methoxyethanol (AR) while stirring at 50 °C for 1 h to get dark yellow solution. After aging at room temperature in air for 24 h, the prepared precursor solution was converted into sol solution and then proper monoethanolamine was added and stirred to avoid cracks during spin coating. All chemical reagents were purchased from Sinopharm Chemical Reagent Co., Ltd.

2.2. CZTSSe Thin Films Preparation. The precursor sol solution was spin coated on molybdenum-coated soda-lime glass (SLG) substrate at 4500 rpm for 30 s followed by annealing at 270 °C for 10 min on a hot plate in air. This coating step was repeated 12 times to get thick CZTS xerogel precursors. After that, the prepared xerogel precursors were annealed at 560 °C (heating rate 15 °C/min) in selenium/N_2 atmosphere (total pressure of about 0.04 MPa during selenization) for 40 min with controlled selenium partial pressure by the temperature of Se powders to obtain desired [S]/([S] + [Se]) ratio(s) and crystallinity.

2.3. CZTSSe Solar Cell Devices Fabrication. The solar cell devices were completed using a chemical bath deposited 70 nm CdS buffer, RF magnetron sputtered 50 nm intrinsic ZnO (i-ZnO), and DC magnetron sputtered 400 nm ITO window layer sequentially. Finally Al was thermally evaporated on ITO layer to form top contact fingers via shadow mask. Each device has a total area of approximately 0.45 cm^2 defined by mechanical scribing.

2.4. Characterization and Analysis. The surface and cross section morphology of thin films were characterized by SEM (FEI Quanta-200 and NOVA NanoSEM 230). The X-ray diffraction (XRD) patterns and Raman spectra were collected by using Rigaku-TTR III X and Jobin-Yvon LabRAM HR-800 (514 nm excitation), respectively. Energy dispersive spectrometry (EDS, EDAX-GENSIS60S in NOVA NanoSEM 230) was used to check the elemental composition and its distribution. An FEI Tecnai G2 equipped with EDS detector was used for the transmission electron microscopy (TEM) analyses. Current density–voltage (J–V) characterization for solar cells were performed

DOI: 10.1021/acsami.5b01151
ACS Appl. Mater. Interfaces 2015, 7, 14376–14383

using Xe-based light source solar simulator (Newport, 91160 and KEITHLEY 2400) to provide simulated 1 sun AM 1.5G illumination which was calibrated with a standard Si reference cell, traceable to the National Renewable Energy Laboratory. The external quantum efficiency (EQE) was measured using a chopped monochromator beam and lock-in amplifier, with calibration into the NIR by Si and Ge diodes measurements (QEX10 spectral response system from PV measurements, Inc.). Time-resolved photoluminescence (TRPL) measurement was performed on device using the time-correlated single photon counting (TCSPC) technique (Microtime200, Picoquant) at a wavelength of 1200 nm and room temperature. The excitation is a 467 nm laser with tunable repetition.

3. RESULTS AND DISUSSION

Top view SEM image of a typical CZTSSe absorber with atomic ratio of Cu/(Zn + Sn) of 0.85, Zn/Sn of 1.00, and [S]/([S] + [Se]) of 0.25 determined by EDS analysis is depicted in Figure 1a, and low-magnification SEM images are presented in Figure S1 (Supporting Information). The CZTSSe film has a relatively dense structure consisting of large grains with a size range of 1−2 μm. Grain sizes up to 3 μm can also be detected. It should be remarked that between the large grains, smaller grains are observable. EDS mapping measurements exhibited in Figure S2 (Supporting Information) show that some small grain regions show slightly stronger sulfur signal than their surroundings, which may be associated with smaller grain size due to less Se incorporation and, thus, lower volume expansion during selenization. All metal elements are homogeneously distributed due to their molecular level mixing with S in the sol−gel process and probably suggests inhomogeneous substitution of Se for S in selenization the process. As the nonuniformity of chalcolgen elements will have great impacts on resulting V_{oc} and efficiency, Raman mapping technology representing [S]/([S] + [Se]) ratio distribution was employed to more precisely assess the degree of this fluctuation of chalcolgen elements (i.e., [S]/([S] + [Se])). Before mapping, a representative Raman spectrum of the CZTSSe absorber was measured for phase identification and purity check first, as shown in Figure 1b. For this sample with intermediate [S]/([S] + [Se]) value, the main peaks from A1 mode of anion vibrations in both selenide CZTSe and sulfide CZTS[27] are presented but deviate toward one other. This coexistence of both groups of bands (i.e., a bimodal behavior) has also been observed for the chalcopyrite $Cu(In,Ga)(S,Se)_2$ material system[28,29] and can be explained in terms of the large mass difference between these two types of anion and the resulting substantial difference between the frequencies of the respective phonons. [S]/([S] + [Se]) ratio calculated from the ratio of the peak intensity for sulfide (~327 cm^{-1}) and selenide (~201 cm^{-1}) peaks after background subtracting is 0.21, correlating well with that determined by EDS. Moreover, no evidence of other possible binary (Cu_2S, CuS_2, ZnS, ZnSe, SnS, SnSe, etc.) or ternary (Cu_2SnS_3 and Cu_2SnSe_3) secondary phases[30−32] can be observed from the prepared CZTSSe absorber. Then the distribution of [S]/([S] + [Se]) ratio is characterized by Raman mapping measurement at a 20 × 20 μm area (441 points), as illustrated in Figure 1c. Although some small regions appear to have higher [S]/([S] + [Se]) ratio, all [S]/([S] + [Se]) ratios are concentrated in a very narrow range from 0.193 to 0.220, and the standard deviation of [S]/([S] + [Se]) ratio distribution by a statistical analysis of the data is only 2% (mean value 0.205 with standard deviation 0.004), suggesting an acceptable distribution homogeneity. Although, the slight lateral fluctuations in [S]/([S] + [Se]) ratio and resulting band gap may still considerably degrade the achievable efficiency of solar cells.[33,34] Therefore, further optimization on selenization process to improve lateral uniformity is needed.

Cross-sectional SEM (CZTSSe device) and TEM (absorber, bright field) images are shown in Figure 2a,b. It is shown that

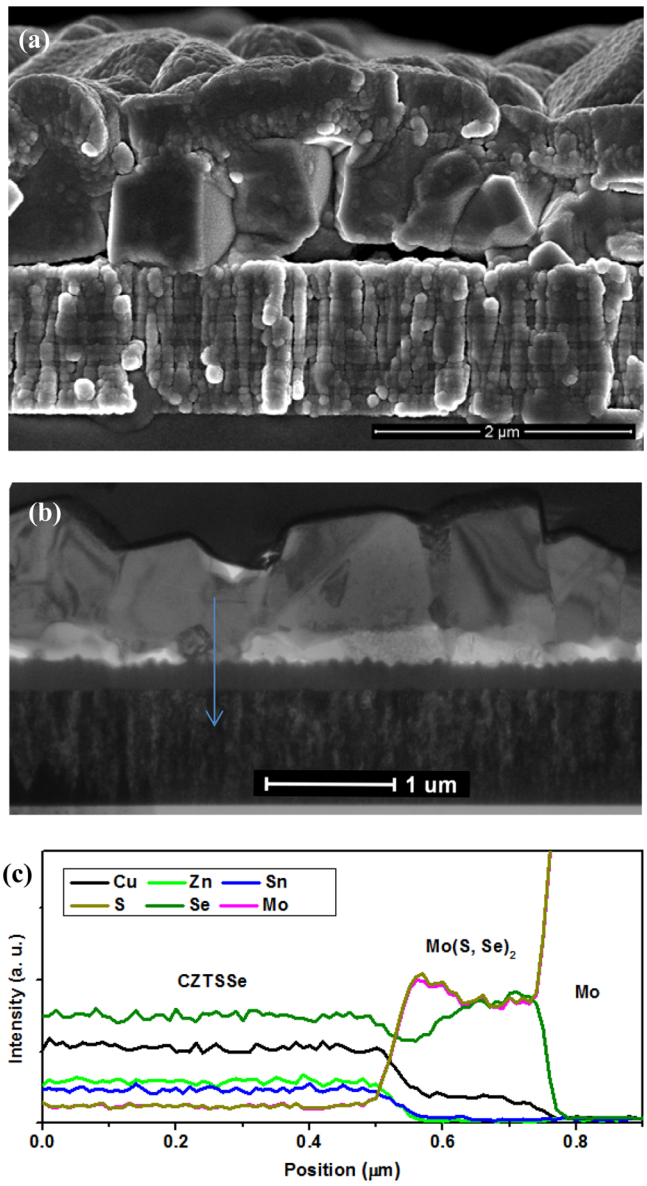

Figure 2. (a) SEM cross section of the typical CZTSSe device. (b) Bright field TEM cross section of typical CZTSSe absorber. (c) Elemental profiles determined by EDS line scan along the blue arrow from absorber to Mo in panel b.

the absorber is composed of mainly large grains spanning the entire layer with thickness of approximately 1 μm. Again, few smaller grains between large grains are observed, leading to the uneven thickness. The carbon-rich or fine grain bottom layer frequently observed in absorbers synthesized by solution processes using organic solvent cannot be found here, while a lot of isolated voids are visible at the bottom part of the absorber. Typical compositional profiling by EDS line scan (Figure 2c) demonstrates uniform elemental distribution along the thickness direction. The SEM and TEM data highlight a $Mo(S,Se)_2$ interfacial layer with a thickness of nearly 300 nm

DOI: 10.1021/acsami.5b01151
ACS Appl. Mater. Interfaces 2015, 7, 14376−14383

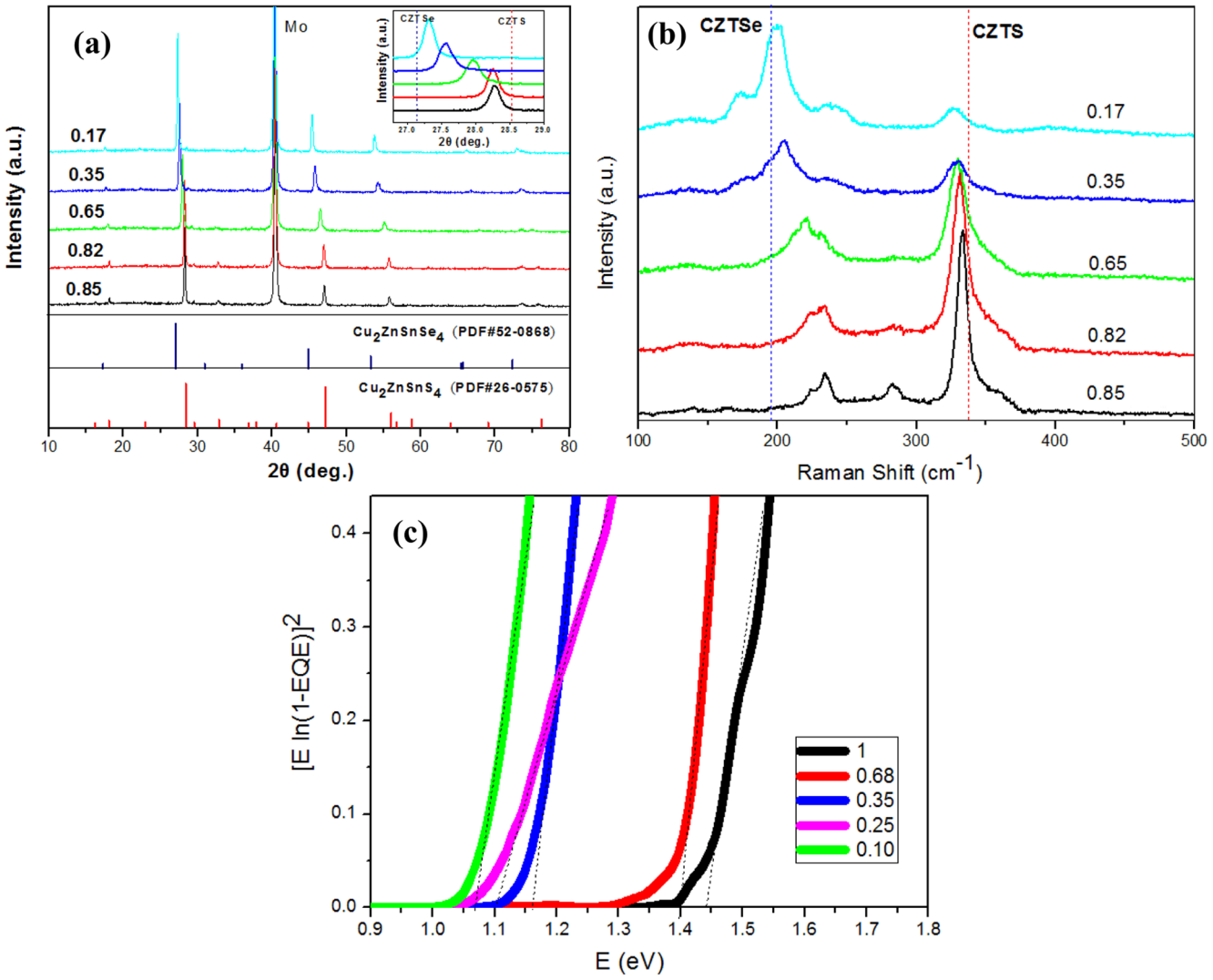

Figure 3. (a) XRD and (b) Raman spectra of the CZTSSe absorbers with varying [S]/([S] + [Se]) ratios (determined by EDS); (a, inset) magnified view of (112) peaks. (c) Band gap calculated from EQE measurements of the device with varying [S]/([S] + [Se]) ratios.

between CZTSSe absorber layer and Mo, as is more evident in EDS composition profiling. The $Mo(S,Se)_2$ interfacial layer may facilitate an electrical quasi-ohmic contact and improve the adhesion of CZTS(e) to Mo back contact[35] but leads to high series resistance and, accordingly, deteriorates the fill factor and the resulting device efficiency if not thin enough,[36,37] similar to the case of CIGSe solar cells.[38] The 300 nm $Mo(S,Se)_2$ layer is considerably thick compared with those in some devices with efficiency higher than 9%.[1−3,7]

As an absorber material, CZTSSe possesses a direct band gap in the range of ∼1.0 eV (CZTSe) to ∼1.5 eV (CZTS), depending upon the [S]/([S] + [Se]) ratio. Tailoring the band gap and its effects on device performance are of great interest. On the basis of theoretical calculations, the optimum band gap for terrestrial single-junction solar cell is around 1.4 eV. One would expect the larger band gap absorbers of the kesterite system to result in higher efficiency, but this is not the case; most of the efficiencies achieved by CZTS or high sulfur-containing CZTSSe absorber are considerably lower than those achieved by high selenium-containing absorber. For instance, the band gap of kesterite absorber in record efficiency is 1.13 eV.[1] Experimentally, Duan et al.[39] reported that when enlarging the band gap of the absorber by increasing its sulfur content, the V_{oc} increases, but the overall efficiency is reduced, as reflected by large V_{oc} deficit and poor carrier collection due to deeper defect energy level and higher defect density. The capability to adjust the [S]/([S] + [Se]) ratio and resulting band gap is crucial to achieve high efficiency solar cells and has been demonstrated here by controlling the temperature of solid selenium source and accordingly the partial pressure of selenium vapor. Figure 3a shows the XRD patterns for several CZTSSe absorbers with varying [S]/([S] + [Se]) ratios. All samples display the presence of several peaks between the ones for the CZTSe (PDF #52-0868) and CZTS (PDF #26-0575) phases, which allows us to believe the formation of kesterite CZTSSe. From the magnified view of (112) peaks in the inset of Figure 3a, the peak position shifts to smaller 2θ values as the [S]/([S] + [Se]) ratio decreases due to the increase in lattice parameters when larger Se atoms (1.98 Å) replace the smaller S atoms (1.84 Å), and accordingly, the interplanar spacing of (112) plane calculated by Bragg equation increases linearly (Figure S3a, Supporting Information), consistent with other reports.[40] Raman spectra of these absorbers in Figure 3b show that the A1 mode peaks shift toward each other linearly (Figure S3b, Supporting Information) with some noticeable peak broadening with [S]/([S] + [Se]) ratio away from both pure

DOI: 10.1021/acsami.5b01151
ACS Appl. Mater. Interfaces 2015, 7, 14376−14383

sulfide (338 cm^{-1}) and selenide (197 cm^{-1}) side, following the similar trend in other reports.[17,41] Moreover, combining XRD and Raman data, no secondary phases can be identified for all absorbers. The band gap values calculated from external quantum efficiency (EQE) of the solar cell devices using absorbers with the [S]/([S] + [Se]) ratios of 0.26, 0.35, and 0.68 are 1.10, 1.16, and 1.40 eV, respectively, as seen in Figure 3c. The band gap 1.43 eV of sulfide CZTS by sol−gel and sulfurization process[22] is also given here for a reference. These results exhibit the ability and flexibility of our process to tune the band gap of CZTSSe absorber.

Figure 4 illuminates the typical current density−voltage (J−V) characteristic curves for devices fabricated using absorbers

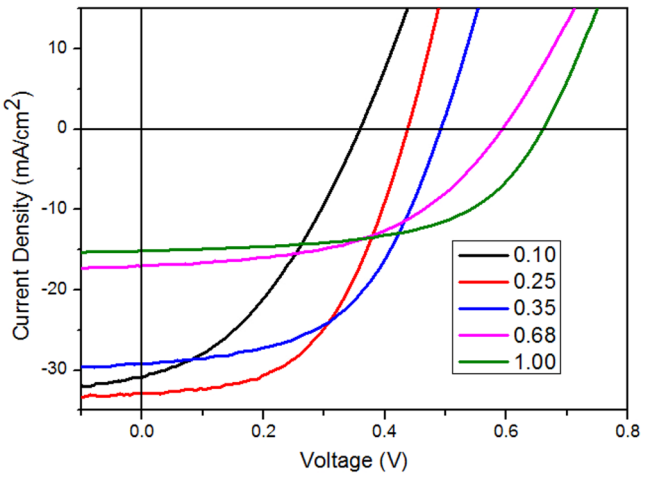

Figure 4. Current density−voltage (J−V) data of the devices using CZTSSe aborbers with various [S]/([S] + [Se]) ratios (determined by EDS).

with different [S]/([S] + [Se]) ratios from 0.1 to 1. The performance parameters deduced from J−V measurements are summarized in Table 1. In order to make the comparison reliable, a statistical treatment is very necessary[42] and is shown in Figure S4 (Supporting Information). As the [S]/([S] + [Se]) ratio increases, the open-circuit voltage (V_{oc}) rises, consistent with its enlarged band gap but the V_{oc} deficit shows an increase trend, revealing that higher [S]/([S] + [Se]) ratio not only enlarges band gap but also leads to more severe recombination. This behavior is in good agreement with previous reports[39,43] and has been attributed to the deep defect energy level and high bulk defect density of the sulfur-rich absorber.[39] The devices fabricated using absorbers with low [S]/([S] + [Se]) ratios have much larger short-circuit current density (J_{sc}) owing to low band gap having enhanced light harvesting in longer wavelength region. High efficiencies above 7% can be achieved for device using absorber with low [S]/([S] + [Se]) ratios (0.25 and 0.35, for example). Note that when [S]/([S] + [Se]) of the absorber is <0.1 the fabricated device also shows large Voc deficit and decreased efficiency. This is because to obtain such high Se content usually requires extremely high Se partial pressure in the selenization process, during which absorber microstructure has been deteriorated showing rather rough and incompact morphology (very low shunt resistance) and very thicker $Mo(S,Se)_2$ interfacial layer was formed (~500 nm, high series resistance) as seen from the cross-sectional SEM image in Figure S5 (Supporting Information). Besides, the deterioration in microstructure and too much Se incorporation causing excess volume expansion may introduce defects leading to recombination and loss in V_{oc}. Good reproducibility is demonstrated from several batches of devices fabricated under slightly varying conditions with efficiencies above 7%. To check large-area film uniformity, we present a typical set of J−V curves from nine devices on the same substrate in Figure S6 (Supporting Information). Efficiencies in the range of 7−8% with an average of 7.47% and standard deviation of 0.31 percentage points are achieved, revealing good large area uniformity. These results show that this sol−gel based route provides a reliable way to fabricate structural and optoelectronic property-controlled CZTSSe absorbers and is very promising for large-scale production of kesterite CZTSSe solar cells.

Figure 5 depicts the J−V characteristics of the highest efficiency device achieved up to date by sol−gel solution

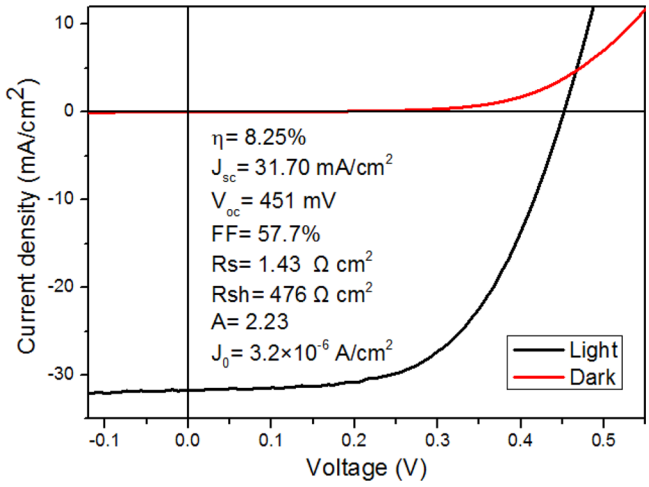

Figure 5. Current density−voltage (J−V) characteristics of the best CZTSSe device with [S]/([S] + [Se]) of 0.25 (determined by EDS) measured in dark and under AM 1.5 simulated sunlight.

method under dark and simulated AM 1.5 illumination. The cross-sectional SEM image has been shown in Figure 2a. This device shows a total area efficiency of 8.25% with an open-circuit voltage of 451 mV, a short-circuit current density of 31.7 mA/cm^2 and fill factor (FF) of 57.7%. Compared to the record CZTSSe device,[1] the efficiency in current device is limited mainly by low FF. The series resistance (R_s), shunt resistance

Table 1. Performance Parameters for Device Using CZTSSe Absorbers with Various [S]/([S] + [Se]) Ratios

[S]/ ([S] + [Se])	η (%)	V_{oc} (mV)	J_{sc} (mA/cm^2)	FF (%)	Eg (eV)	Eg/q−V_{oc} (mV)	R_s (Ω cm^2)	R_{sh} (Ω cm^2)
x = 1.00	5.73	664	15.15	57.0	1.43	766	2.6	545
x = 0.68	5.06	596	17.03	50.0	1.40	804	3.8	320
x = 0.35	7.53	493	29.20	52.3	1.16	667	2.1	254
x = 0.25	7.45	439	32.83	51.6	1.10	661	1.7	306
x = 0.10	4.23	358	30.85	38.3	1.07	712	2.4	90

DOI: 10.1021/acsami.5b01151
ACS Appl. Mater. Interfaces 2015, 7, 14376−14383

(R_{sh}), diode ideality factor (A), and reverse saturation current density (J_0) extracted from the light $J-V$ curves using Sites' method[44] are 1.43 Ω cm^2, 476 Ω cm^2, 2.23 and 3.2 × 10^{-6} A/cm^2, respectively. The R_s, A, and J_0 values are significantly higher than those in record device,[1] which accounts for the low FF. The high series resistance can be reasonably attributed to the presence of lots of voids at the bottom part of the absorber and thick $Mo(S,Se)_2$ interfacial layer between absorber and Mo back contact. By eliminating the undesirable voids and reducing the thickness of $Mo(S,Se)_2$ layer, thereby reducing the R_s, a further boost in CZTSSe device efficiency is highly possible. An A value larger than 2 is characteristic of strong space-charge region (SCR) recombination or the possibility of additional contributions to SCR recombination from trap assisted tunneling,[45,46] both of which can lead to a high J_0.[46]

To gain further insight in device performance, we measured the external quantum efficiency (EQE) of the device, as shown in Figure 6. The integrated short-circuit current density

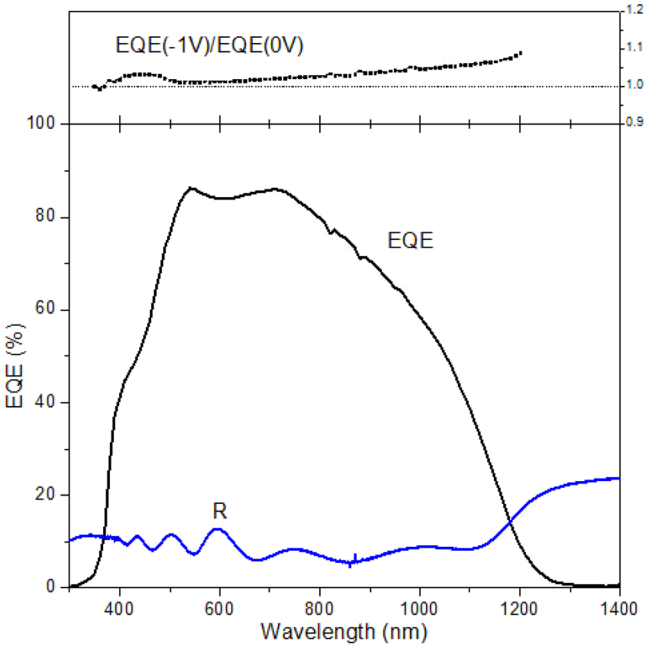

Figure 6. (Bottom) External quantum efficiency (EQE) at 0 V bias and reflectance spectrum of the best CZTSSe device. (Top) EQE ratio at −1 and 0 V bias.

extracted from the EQE data agrees well with that obtained by $J-V$ test under simulated sunlight, and the band gap estimated from the EQE is 1.09 eV. The EQE exceeds 80% in the visible light range; however, it decays at longer wavelength. The lack of long wavelength response reveals a loss of deeply absorbed photons and thereby low carrier collection efficiency, which is examined by the measurement of the ratio of EQE at reverse −1 and 0 V bias, as shown in the top panel of Figure 6. The ratio increases toward long wavelength direction, confirming the recombination for minority carriers occurring in neutral region, that is, the minority carriers generated deep in the absorber by long wavelength photons are difficult to be collected effectively, and a larger depletion width extended into absorber by reverse bias improve the collection efficiency with a resultant increase in EQE. All EQE(−1 V)/EQE(0 V) ratios are above 1 in the whole wavelength range, suggesting strong SCR recombination (interface or near the junction).[20,47] These behaviors are most likely caused by short carrier lifetime compared with CIGS.[43] In addition, from the reflectivity spectrum of the device with an average reflectivity of 9.2% in the range of 300−1200 nm, it is expected that a notable improvement in EQE and resulting J_{sc} can be achieved by the addition of a MgF_2 antireflection coating.

The time-resolved photoluminescence (TRPL) measurement was performed to check the minority carrier lifetime of the device, as shown in Figure 7. The TRPL data do not follow a

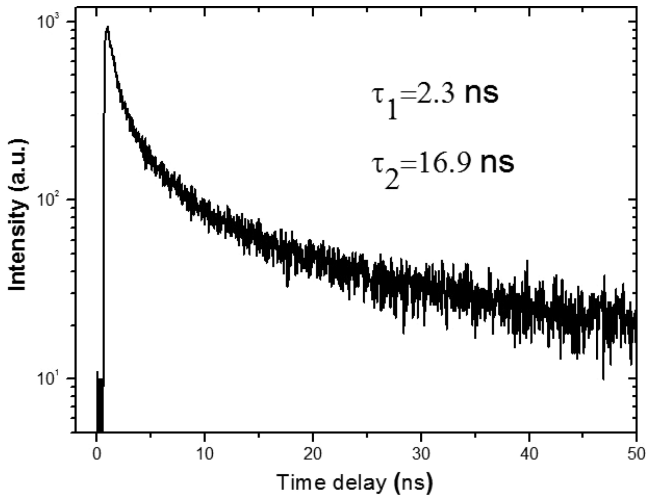

Figure 7. Time-resolved photoluminescence trace carried out on the finished device.

monoexponential decay, implying a varying lifetime as the time scale changes. We use biexponential fitting to analyze the curve as described by Ohnesorge et al.[48] The initial fast decay with a time constant τ_1 of 2.3 ns is ascribed to a radiative recombination process in the high-injection regime immediately after the laser pulse with the optically excited excess carrier concentration.[49] The minority carrier lifetime characterized by the time constant τ_2 is 16.9 ns. This is a relatively long lifetime in CZTSSe system (but still lower than that in CIGS and let alone Si), but device performance is far below the expected level by comparing with the experimental reports[16] and model predictions.[50] This shortfall may be due to some other physical mechanisms that does not affect the measured lifetime.[50] One possible mechanism is the slight lateral nonuniformity in [S]/([S] + [Se]) ratio and resulting band gap fluctuations as revealed by EDS and Raman mapping, which allows significant interface recombination[34] and may partly contribute to the nonlinear behavior the TRPL data, with the TRPL signal having individual contributions from different region with varying lifetimes.[51] On the other hand, the underperformance of the device also implies the necessity to optimize the device fabrication conditions, especially for CdS buffer, contacts and TCO to push efficiency up to 10%. The minority carrier lifetime is still much shorter than the typical tens to hundreds of nanoseconds for high-efficiency CIGS devices[52,53] and needs further improvement.

4. CONCLUSIONS

In summary, we present a simple and facile synthesis of an earth abundant kesterite $Cu_2ZnSn(S,Se)_4$ (CZTSSe) absorbers with large grains, a single phase, and good uniformity using a sol−gel and selenization process. A slight fluctuation with acceptable

DOI: 10.1021/acsami.5b01151
ACS Appl. Mater. Interfaces 2015, 7, 14376−14383

deviation in [S]/([S] + [Se]) ratio has been confirmed by EDS and Raman mapping. The capacity for tuning the structural and optoelectronic properties through the adjustment of [S]/([S] + [Se]) composition by controlling the selenium partial pressure has been demonstrated. The maximum total area efficiency without an antireflection coating of 8.25% has already been achieved based on this process. Relatively low FF is the main limitation for current device performance compared to the record CZTSSe device and is caused by high series resistance and significant interface recombination. Optimization to improve film uniformity, eliminate the voids at the bottom part of the absorber, reduce the $Mo(S,Se)_2$ interfacial layer, and improve device fabrication process is expected to yield further enhancement in efficiency, making this process one of the most promising candidates for fabrication of low-cost, larger-area, high-efficiency kesterite solar cells.

■ ASSOCIATED CONTENT

Supporting Information

SEM top-view images of CZTSSe absorber at low magnifications; EDS element mapping images of CZTSSe absorber; positions of interplnar spacings of (112) plane and A1 mode Raman peaks for sulfide and selenide in CZTSSe absorbers shift with varying [S]/([S] + [Se]); histograms of four device parameters (J_{sc}, V_{oc}, FF, and efficiency) for a set of glass/Mo/CZTSSe/CdS/i-ZnO/ITO cells, composed of 100 devices (20 devices or each [S]/([S] + [Se] ratio value x); cross sectional-SEM image of CZTSSe device using absorber with [S]/([S] + [Se]) ratio of 0.1; and current density−voltage (J−V) data of 9 CZTSSe devices on the same substrate. The Supporting Information is available free of charge on the ACS Publications website at DOI: 10.1021/acsami.5b01151.

■ AUTHOR INFORMATION

Corresponding Authors

*E-mail: liufangyan@csu.edu.cn.
*E-mail: xj.hao@unsw.edu.au.

Notes

The authors declare no competing financial interest.

■ ACKNOWLEDGMENTS

The authors thank Professor Martin Green at The University of New South Wales for helpful discussions on this work. This work was supported by The National Natural Science Foundation of China (Grant No. 51204214). The authors also acknowledge the Australian Government for financial support through the Australian Research Council (ARC). The authors also acknowledge the facilities and the scientific and technical assistance of The Mark Wainwright Analytical Centre (MWAC) at The University of New South Wales.

■ REFERENCES

(1) Wang, W.; Winkler, M. T.; Gunawan, O.; Gokmen, T.; Todorov, T. K.; Zhu, Y.; Mitzi, D. B. Device Characteristics of CZTSSe Thin-Film Solar Cells with 12.6% Efficiency. *Adv. Energy Mater.* **2014**, *4*, 1301465.

(2) Repins, I.; Beall, C.; Vora, N.; DeHart, C.; Kuciauskas, D.; Dippo, P.; To, B.; Mann, J.; Hsu, W.-C.; Goodrich, A.; Noufi, R. Co-evaporated $Cu_2ZnSnSe_4$ Films and Devices. *Sol. Energy Mater. Sol. Cells* **2012**, *101*, 154−159.

(3) Hsu, W. C.; Repins, I.; Beall, C.; DeHart, C.; To, B.; Yang, W. B.; Yang, Y.; Noufi, R. Growth Mechanisms of Co-evaporated Kesterite: A Comparison of Cu-Rich and Zn-Rich Composition Paths. *Prog. Photovoltaics* **2014**, *22*, 35−43.

(4) Shin, B.; Gunawan, O.; Zhu, Y.; Bojarczuk, N. A.; Chey, S. J.; Guha, S. Thin Film Solar Cell with 8.4% Power Conversion Efficiency Using an Earth-Abundant Cu_2ZnSnS_4 Absorber. *Prog. Photovoltaics* **2013**, *21*, 72−76.

(5) Sugimoto, H.; Hiroi, H.; Sakai, N.; Muraoka, S.; Katou, T. Over 8% Efficiency Cu_2ZnSnS_4 Submodules with Ultra-Thin Absorber. *Photovoltaic Specialists Conference (PVSC), 2012 38th IEEE* **2012**, 002997−003000.

(6) Chawla, V.; Clemens, B. Effect of Composition on High Efficiency CZTSSe Devices Fabricated Using Co-sputtering of Compound Targets. *Photovoltaic Specialists Conference (PVSC), 2012 38th IEEE* **2012**, 002990−002992.

(7) Brammertz, G.; Buffière, M.; Oueslati, S.; ElAnzeery, H.; Ben Messaoud, K.; Sahayaraj, S.; Köble, C.; Meuris, M.; Poortmans, J. Characterization of Defects in 9.7% Efficient $Cu_2ZnSnSe_4$−CdS−ZnO Solar Cells. *Appl. Phys. Lett.* **2013**, *103*, 163904.

(8) Jiang, F.; Ikeda, S.; Harada, T.; Matsumura, M. Pure Sulfide Cu_2ZnSnS_4 Thin Film Solar Cells Fabricated by Preheating an Electrodeposited Metallic Stack. *Adv. Energy Mater.* **2013**, *4*, 1301381.

(9) Guo, L.; Zhu, Y.; Gunawan, O.; Gokmen, T.; Deline, V. R.; Ahmed, S.; Romankiw, L. T.; Deligianni, H. Electrodeposited $Cu_2ZnSnSe_4$ Thin Film Solar Cell with 7% Power Conversion Efficiency. *Prog. Photovoltaics* **2014**, *22*, 58−68.

(10) Cao, Y.; Denny, M. S.; Caspar, J. V.; Farneth, W. E.; Guo, Q.; Ionkin, A. S.; Johnson, L. K.; Lu, M.; Malajovich, I.; Radu, D.; Rosenfeld, H. D.; Choudhury, K. R.; Wu, W. High-Efficiency Solution-Processed $Cu_2ZnSn(S,Se)_4$ Thin-Film Solar Cells Prepared from Binary and Ternary Nanoparticles. *J. Am. Chem. Soc.* **2012**, *134*, 15644−15647.

(11) Miskin, C. K.; Yang, W.-C.; Hages, C. J.; Carter, N. J.; Joglekar, C. S.; Stach, E. A.; Agrawal, R. 9.0% Efficient $Cu_2ZnSn(S,Se)_4$ Solar Cells from Selenized Nanoparticle Inks. *Prog. Photovoltaics* **2015**, *23* (5), 654−659.

(12) Guo, Q.; Ford, G. M.; Yang, W.-C.; Hages, C. J.; Hillhouse, H. W.; Agrawal, R. Enhancing the Performance of CZTSSe Solar Cells with Ge Alloying. *Sol. Energy Mater. Sol. Cells* **2012**, *105*, 132−136.

(13) Zhong, J.; Xia, Z.; Zhang, C.; Li, B.; Liu, X.; Cheng, Y.-B.; Tang, J. One-Pot Synthesis of Self-Stabilized Aqueous Nanoinks for $Cu_2ZnSn(S,Se)_4$ Solar Cells. *Chem. Mater.* **2014**, *26*, 3573−3578.

(14) Todorov, T. K.; Reuter, K. B.; Mitzi, D. B. High-Efficiency Solar Cell with Earth-Abundant Liquid-Processed Absorber. *Adv. Mater.* **2010**, *22*, E156−E159.

(15) Barkhouse, D. A. R.; Gunawan, O.; Gokmen, T.; Todorov, T. K.; Mitzi, D. B. Device Characteristics of a 10.1% Hydrazine-processed $Cu_2ZnSn(Se,S)_4$ Solar Cell. *Prog. Photovoltaics* **2012**, *20*, 6−11.

(16) Todorov, T. K.; Tang, J.; Bag, S.; Gunawan, O.; Gokmen, T.; Zhu, Y.; Mitzi, D. B. Beyond 11% Efficiency: Characteristics of State-of-the-Art $Cu_2ZnSn(S,Se)_4$ Solar Cells. *Adv. Energy Mater.* **2013**, *3*, 34−38.

(17) Yang, W.; Duan, H.-S.; Bob, B.; Zhou, H.; Lei, B.; Chung, C.-H.; Li, S.-H.; Hou, W. W.; Yang, Y. Novel Solution Processing of High-Efficiency Earth-Abundant $Cu_2ZnSn(S,Se)_4$ Solar Cells. *Adv. Mater.* **2012**, *24*, 6323−6329.

(18) Jiang, M. L.; Lan, F.; Yan, X. Z.; Li, G. Y. $Cu_2ZnSn(S_{1-x}Se_x)_4$ Thin Film Solar Cells Prepared by Water-based Solution Process. *Phys. Status Solidi RRL* **2014**, *8*, 223−227.

(19) Wang, G.; Zhao, W.; Cui, Y.; Tian, Q.; Gao, S.; Huang, L.; Pan, D. Fabrication of a $Cu_2ZnSn(S,Se)_4$ Photovoltaic Device by a Low-Toxicity Ethanol Solution Process. *ACS Appl. Mater. Inter* **2013**, *5*, 10042−10047.

(20) Xin, H.; Katahara, J. K.; Braly, I. L.; Hillhouse, H. W. 8% Efficient $Cu_2ZnSn(S,Se)_4$ Solar Cells from Redox Equilibrated Simple Precursors in DMSO. *Adv. Energy Mater.* **2014**, *4*, 1301823.

(21) Su, Z.; Sun, K.; Han, Z.; Cui, H.; Liu, F.; Lai, Y.; Li, J.; Hao, X.; Liu, Y.; Green, M. A. Fabrication of Cu_2ZnSnS_4 Solar Cells with 5.1% Efficiency via Thermal Decomposition and Reaction Using a Non-toxic Sol−Gel Route. *J. Mater. Chem. A* **2014**, *2*, 500−509.

DOI: 10.1021/acsami.5b01151
ACS Appl. Mater. Interfaces 2015, 7, 14376−14383

(22) Zhang, K.; Su, Z.; Zhao, L.; Yan, C.; Liu, F.; Cui, H.; Hao, X.; Liu, Y. Improving the Conversion Efficiency of Cu_2ZnSnS_4 Solar Cell by Low Pressure Sulfurization. *Appl. Phys. Lett.* **2014**, *104*, 141101.
(23) Kwon, S. G.; Hyeon, T. Colloidal Chemical Synthesis and Formation Kinetics of Uniformly Sized Nanocrystals of Metals, Oxides, and Chalcogenides. *Acc. Chem. Res.* **2008**, *41*, 1696−1709.
(24) Niederberger, M. Nonaqueous Sol−Gel Routes to Metal Oxide Nanoparticles. *Acc. Chem. Res.* **2007**, *40*, 793−800.
(25) Maeda, K.; Tanaka, K.; Fukui, Y.; Uchiki, H. Influence of H_2S Concentration on the Properties of Cu_2ZnSnS_4 Thin Films and Solar Cells Prepared by Sol−Gel Sulfurization. *Sol. Energy Mater. Sol. Cells* **2011**, *95*, 2855−2860.
(26) Tanaka, K.; Fukui, Y.; Moritake, N.; Uchiki, H. Chemical Composition Dependence of Morphological and Optical Properties of Cu_2ZnSnS_4 Thin Films Deposited by Sol−Gel Sulfurization and Cu_2ZnSnS_4 Thin Film Solar Cell Efficiency. *Sol. Energy Mater. Sol. Cells* **2011**, *95*, 838−842.
(27) Altosaar, M.; Raudoja, J.; Timmo, K.; Danilson, M.; Grossberg, M.; Krustok, J.; Mellikov, E. $Cu_2Zn_{1-x}Cd_xSn(Se_{1-y}S_y)_4$ Solid Solutions As Absorber Materials for Solar Cells. *Phys. Status Solidi A* **2008**, *205*, 167−170.
(28) Palm, J.; Jost, S.; Hock, R.; Probst, V. Raman Spectroscopy for Quality Control and Process Optimization of Chalcopyrite Thin Films and Devices. *Thin Solid Films* **2007**, *515*, 5913−5916.
(29) Bacewicz, R.; Gebicki, W.; Filipowicz, J. Raman Scattering in $CuInS_{2x}$ $Se_{2(1-x)}$ Mixed Crystals. *J. Phys.: Condens. Matter* **1994**, *6*, L777.
(30) Vigil-Galán, O.; Espíndola-Rodríguez, M.; Courel, M.; Fontané, X.; Sylla, D.; Izquierdo-Roca, V.; Fairbrother, A.; Saucedo, E.; Pérez-Rodríguez, A. Secondary Phases Dependence on Composition Ratio in Sprayed Cu_2ZnSnS_4 Thin Films and Its Impact on the High Power Conversion Efficiency. *Sol. Energy Mater. Sol. Cells* **2013**, *117*, 246−250.
(31) Ahmadi, M.; Pramana, S. S.; Batabyal, S. K.; Boothroyd, C.; Mhaisalkar, S. G.; Lam, Y. M. Synthesis of Cu_2SnSe_3 Nanocrystals for Solution Processable Photovoltaic Cells. *Inorg. Chem.* **2013**, *52*, 1722−1728.
(32) Fernandes, P. A.; Sousa, M. G.; Salome, P. M. P.; Leitao, J. P.; da Cunha, A. F. Thermodynamic Pathway for the Formation of SnSe and $SnSe_2$ Polycrystalline Thin Films by Selenization of Metal Precursors. *CrystEngComm* **2013**, *15*, 10278−10286.
(33) Rau, U.; Werner, J. H. Radiative Efficiency Limits of Solar Cells with Lateral Band-gap Fluctuations. *Appl. Phys. Lett.* **2004**, *84*, 3735−3737.
(34) Werner, J. H.; Mattheis, J.; Rau, U. Efficiency Limitations of Polycrystalline Thin Film Solar Cells: Case of $Cu(In,Ga)Se_2$. *Thin Solid Films* **2005**, *480−481*, 399−409.
(35) Liu, F.; Sun, K.; Li, W.; Yan, C.; Cui, H.; Jiang, L.; Hao, X.; Green, M. A. Enhancing the Cu_2ZnSnS_4 Solar Cell Efficiency by Back Contact Modification: Inserting a Thin TiB_2 Intermediate Layer at Cu_2ZnSnS_4/Mo Interface. *Appl. Phys. Lett.* **2014**, *104*, 051105.
(36) Shin, B.; Bojarczuk, N. A.; Guha, S. On the Kinetics of $MoSe_2$ Interfacial Layer Formation in Chalcogen-based Thin Film Solar Cells with a Molybdenum Back Contact. *Appl. Phys. Lett.* **2013**, *102*, 091907−4.
(37) Scragg, J. J.; Kubart, T.; Wätjen, J. T.; Ericson, T.; Linnarsson, M. K.; Platzer-Björkman, C. Effects of Back Contact Instability on Cu_2ZnSnS_4 Devices and Processes. *Chem. Mater.* **2013**, *25*, 3162−3171.
(38) Zhu, X.; Zhou, Z.; Wang, Y.; Zhang, L.; Li, A.; Huang, F. Determining Factor of $MoSe_2$ Formation in $Cu(In,Ga)Se_2$ Solar Cells. *Sol. Energy Mater. Sol. Cells* **2012**, *101*, 57−61.
(39) Duan, H.-S.; Yang, W.; Bob, B.; Hsu, C.-J.; Lei, B.; Yang, Y. The Role of Sulfur in Solution-Processed $Cu_2ZnSn(S,Se)_4$ and its Effect on Defect Properties. *Adv. Funct. Mater.* **2013**, *23*, 1466−1471.
(40) Cao, Y.; Xiao, Y.; Jung, J.-Y.; Um, H.-D.; Jee, S.-W.; Choi, H. M.; Bang, J. H.; Lee, J.-H. Highly Electrocatalytic $Cu_2ZnSn(S_{1-x}Se_x)_4$ Counter Electrodes for Quantum-Dot-Sensitized Solar Cells. *ACS Appl. Mater. Inter* **2013**, *5*, 479−484.
(41) Mitzi, D. B.; Todorov, T. K.; Gunawan, O.; Min, Y.; Qing, C.; Wei, L.; Reuter, K. B.; Kuwahara, M.; Misumi, K.; Kellock, A. J.; Chey, S. J.; de Monsabert, T. G.; Prabhakar, A.; Deline, V.; Fogel, K. E. Towards Marketable Efficiency Solution-Processed Kesterite and Chalcopyrite Photovoltaic Devices. *Photovoltaic Specialists Conference (PVSC), 2010 35th IEEE* **2010**, 000640−000645.
(42) Luber, E. J.; Buriak, J. M. Reporting Performance in Organic Photovoltaic Devices. *ACS Nano* **2013**, *7*, 4708−4714.
(43) Mitzi, D. B.; Gunawan, O.; Todorov, T. K.; Wang, K.; Guha, S. The Path Towards a High-Performance Solution-Processed Kesterite Solar Cell. *Sol. Energy Mater. Sol. Cells* **2011**, *95*, 1421−1436.
(44) Sites, J. R.; Mauk, P. H. Diode Quality Factor Determination for Thin-Film Solar Cells. *Sol. Cells* **1989**, *27*, 411−417.
(45) Rau, U. Tunneling-Enhanced Recombination in $Cu(In,Ga)Se_2$ Heterojunction Solar Cells. *Appl. Phys. Lett.* **1999**, *74*, 111−113.
(46) Contreras, M. A.; Ramanathan, K.; AbuShama, J.; Hasoon, F.; Young, D. L.; Egaas, B.; Noufi, R. Diode Characteristics in State-of-the-Art ZnO/CdS/$Cu(In_{1-x}Ga_x)Se_2$ Solar Cells. *Prog. Photovoltaics* **2005**, *13*, 209−216.
(47) Hegedus, S. S.; Shafarman, W. N. Thin-Film Solar Cells: Device Measurements and Analysis. *Prog. Photovoltaics* **2004**, *12*, 155−176.
(48) Ohnesorge, B.; Weigand, R.; Bacher, G.; Forchel, A.; Riedl, W.; Karg, F. H. Minority-carrier Life Time and Efficiency of $Cu(In,Ga)Se_2$ Solar Cells. *Appl. Phys. Lett.* **1998**, *73*, 1224−1226.
(49) Gunawan, O.; Todorov, T. K.; Mitzi, D. B. Loss Mechanisms in Hydrazine-Processed $Cu_2ZnSn(Se,S)_4$ Solar Cells. *Appl. Phys. Lett.* **2010**, *97*.
(50) Repins, I. L.; Moutinho, H.; Choi, S. G.; Kanevce, A.; Kuciauskas, D.; Dippo, P.; Beall, C. L.; Carapella, J.; DeHart, C.; Huang, B.; Wei, S. H. Indications of Short Minority-carrier Lifetime in Kesterite Solar Cells. *J. Appl. Phys.* **2013**, *114*, 084507.
(51) Bag, S.; Gunawan, O.; Gokmen, T.; Zhu, Y.; Mitzi, D. B. Hydrazine-Processed Ge-Substituted CZTSe Solar Cells. *Chem. Mater.* **2012**, *24*, 4588−4593.
(52) Metzger, W. K.; Repins, I. L.; Contreras, M. A. Long Lifetimes in High-efficiency $Cu(In,Ga)Se_2$ Solar Cells. *Appl. Phys. Lett.* **2008**, *93*, 022110.
(53) Repins, I. L.; Metzger, W. K.; Perkins, C. L.; Li, J. V.; Contreras, M. A. Correlation Between Measured Minority-Carrier Lifetime and $Cu(In,Ga)Se_2$ Device Performance. *IEEE Trans. Electron Devices* **2010**, *57*, 2957−2963.

DOI: 10.1021/acsami.5b01151
ACS Appl. Mater. Interfaces 2015, 7, 14376−14383